NM WRRI Student Water Research Grant Final Report

Progress Report due November 1, 2019
Draft Final Report due April 30, 2020
Final Report due May 31, 2020

1. **Student Researcher**: Jiuling Yu
   Faculty Advisor: Dr. Hongmei Luo

2. **Project title**:
Wastewater-Treatment Algae-Derived Hydrochar for Heavy Metal Adsorption and Recycling

3. **Description of research problem and research objectives.**

3.1 Research problem
Water contamination caused by heavy metals has been a severe environmental issue in New Mexico (NM), because heavy metals are being released into groundwater by wind or water erosion from over 15,000 abandoned mines in NM. Additionally, the waterways in NM were affected by Gold King Mine waste water spill in 2015, which highly increased the concentrations of heavy metals, such as lead (Pb), in the water. Excess lead in the groundwater could be harmful to neurological, cardiovascular and renal systems of human beings[1]. Therefore, it is imperative to explore an effective technique to remove Pb(II) from groundwater. Adsorption is an attractive strategy on removal of Pb(II) due to its low-cost and simple operation condition. Recently, carbon derived from abundant and renewable biomass has been considered as a high-efficiency adsorbent to remove Pb(II) in the wastewater treatment [2, 3]. Among them, algae is an ideal renewable energy resource due to its high-rate growth, strong CO_2-mitigation potential, good adaptability in variable climatic conditions and large possibility of large-scale artificial cultivation [4]. Hence, hydrochar derived from wastewater-treatment filamentous algae is proposed to be an effective adsorbent for Pb(II) removal. Nevertheless, it remains challenging to dispose the Pb-adsorbed hydrochar in a sustainable way. Inspired by others' work, Pb-adsorbed hydrochar is further developed to be the anode materials in lithium-ion batteries (LIBs).

3.2 Research objectives
The objective of our research is to (1) investigate the effects of pretreatments (oil extraction and CO_2 activation) on the adsorption capacity of Pb, (2) explore the adsorption capacity on Pb(II) for waste hydrochar derived from hydrothermal liquefaction (HTL)-algae, and (3) evaluate the feasibility of recycle of Pb-adsorbed hydrochar as anode materials in LIBs.

4. **Description of methodology employed.**

Hydrochar by hydrothermal processing of wastewater-treatment algae was provided by Dr. Catherine Brewer's group at NMSU. Two types of pretreatments (oil-extracted process and CO_2 activation) were performed before adsorption experiments. To evaluate the adsorption capacity of Pb(II), 1000 mg/L Pb(II) solution was firstly prepared by dissolving certain amount of $Pb(NO_3)_2$ in DI water as the stock lead solution. The targeted solutions were prepared by diluting stock solution with a certain ratio of DI water. The adsorption capacity was calculated by the following equation:

$$q_e = \frac{(C_0 - C_e) \times V}{W} \qquad \text{Eq. (1)}$$

where q_e (mg Pb g^{-1} adsorbent) is the adsorption capacity at equilibrium, C_0 (mg L^{-1}) and C_e (mg L^{-1}) are the initial concentration and equilibrium concentrations, respectively, V (L) is the volume of Pb(II) solution, and W (g) is mass of adsorbent added.

The Langmuir [5] and the Freundlich [6] adsorption models were compared with the adsorption data, using the linearized forms [7], here:

$$\text{Langmuir} \qquad \frac{C_e}{q_e} = \frac{1}{K_L q_m} + \frac{C_e}{q_m} \qquad \text{Eq. (2)}$$

$$\text{Freundlich} \qquad \ln q_e = \ln K_F + \frac{1}{n} \ln C_e \qquad \text{Eq. (3)}$$

where C_e (mg L^{-1}) is the equilibrium Pb concentration in solution, q_e (mg g^{-1}) is Pb(II) adsorbed at equilibrium, q_m (mg g^{-1}) is the maximum adsorption capacity, K_L (L mg^{-1}) is the Langmuir constant, K_F (mg g^{-1}) is the Freundlich constant related to adsorption capacity, n is the constant related to energy.

The electrochemical experiments were carried out using CR2025 coin cells with as-obtained working electrode, separator, and lithium chip in an argon-filled glovebox. 1 M $LiPF_6$ in a mixture of ethylene carbonate (EC) and dimethyl carbonate (DMC) (1:1 v/v) was used as the electrolyte.

5. Description of results; include findings, conclusions, and recommendations for further research.

To make a clear comparison of hydrochar treated by different pretreatments, the operating conditions with abbreviated names are listed in Table 1.

Table 1. Summary of pretreated hydrochar with their abbreviated names.

Pretreatment condition	Abbreviation
Unextracted/inactivated	U_char
Unextracted/activated	UA_char
Extracted/inactivated	EN_char
Extracted/activated	EA_char

The composition of algae biomass feedstock and original untreated-hydrochar (U_char) obtained from HTL without any pretreatment are shown in Table 2. It's clear to observe that algae biomass feedstock has a lower ash content than U_char, while its carbon content is much higher than that of U_char. The possible reason is that the relatively high temperature of 350 °C in the HTL process is apt to form the liquid phase of bio-crude oil, resulting in decomposing partial solid carbon into the liquid phase and concentrating the ash into the solid phase. Therefore, U_char shows the higher ash content and lower carbon content after processing HTL, leading to the lower HHV than algae feedstock. It should be pointed that the carbon contents of both feedstock (46.6 wt.%) and U_char (46.4 wt.%) are almost equal when considering the composition proportion on the ash-free basis samples. Another fact is O/C ratio of U_char (0.85) is higher than that of feedstock (0.75), which implies the biomass feedstock decomposes incompletely during HTL process [8].

Table 2. Composition of algae biomass feedstock and U_char (Average value of duplication ± standard deviation).

	Algae biomass feedstock	U_char
Proximate analysis (dry basis)		
Ash content / wt.%	13.5 ± 0.4	41.8 ± 0.5
HHV / MJ kg^{-1}	26.2 ± 0.3	20.3 ± 0.5
Elemental analysis wt.% (dry basis)		
Carbon	40.3 ± 1.5	27.0 ± 0.3
Hydrogen	6.1 ± 0.2	1.7 ± 0.3
Nitrogen	7.1 ± 0.5	2.7 ± 0.1
Sulfur	2.6 ± 0.3	3.9 ± 1.5
Oxygen[a]	30.4 ± 1.7	22.9 ± 1.6

[a] by difference
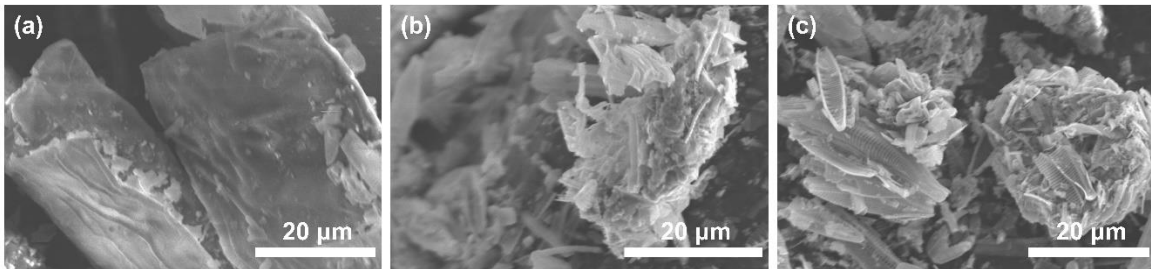
Figure 1. SEM images of (a) Algae biomass feedstock; (b) Unextracted/inactivated hydrochar (U_char); and (c) Unextracted/activated hydrochar (UA_char).

The surface structural differences are presented by SEM images, as shown in Figure 1. Obviously, the surface structure of filamentous algae biomass in Figure 1(a) is quite different than the other two hydrochar samples. Filamentous algae biomass shows a flat and smooth surface in a rectangular-type structure, which looks like the fragment of algae. Whereas, irregular aggregation consisting of numbers of small cracks are observed in Figure 1(b) and 1(c), due to the volatiles release and decomposition during HTL treatment [9].
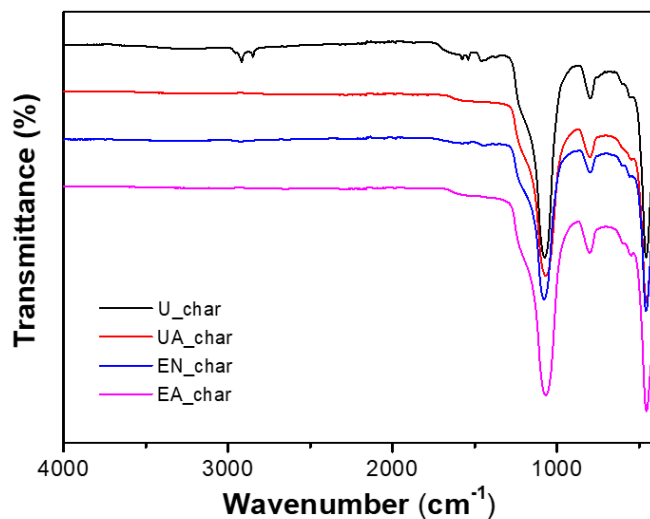
Figure 2. FT-IR spectra of U_char, UA_char, EN_char, and EA_char.

FT-IR spectra of four types of hydrochar (U_char, UA_char, EN_char, and EA_char) are shown in Figure 2 to reveal the functional groups on the surface. From Figure 2, three strong peaks at 1075, 797 and 456 cm^{-1} can be observed in all hydrochar. All these peaks are attributed to the existence of silica in the hydrochar [10].
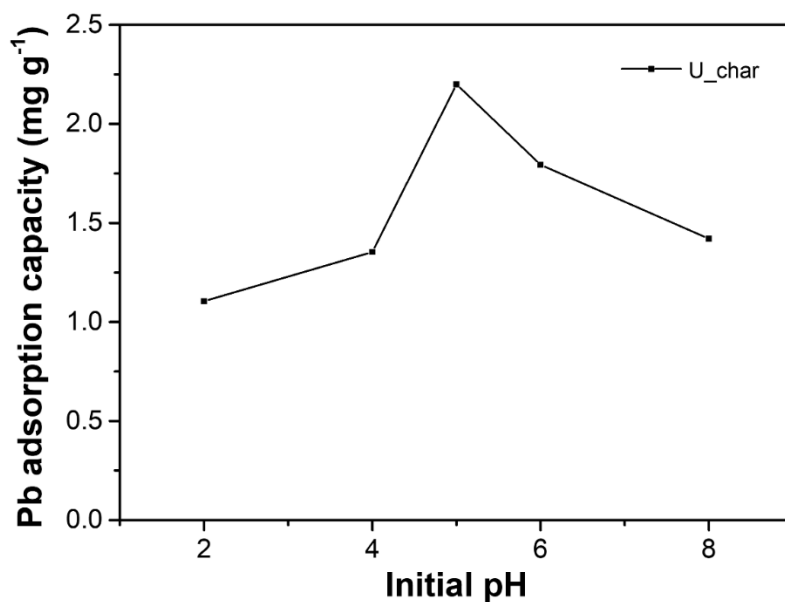
Figure 3. Effect of initial solution pH on Pb(II) adsorption onto U_char. Adsorption conditions were 4 g L^{-1} adsorbent and room temperature.

In metal ion adsorption, there is a strong correlation between solution pH and formation of metal ions and surface charges on the adsorbent [11], and the degree of ionization for the adsorbate [12]. The effect of initial pH on Pb(II) adsorption onto U_char over the pH range of 2.0-8.0 is shown in Figure 3. The adsorption capacity increases with pH from 2.0 to 5.0 and then decreases after pH 5.0, with the maximum adsorption capacity of 2.20 mg g^{-1} at pH 5.0. At pH < 5.0, Pb(II) speciation

favors the ionic state, resulting in a competition between Pb(II) and protons in the solution for sites on the hydrochar surface [13]. Increasing pH value deprotonates occupied active sites, which is beneficial to Pb^{2+} adsorption, leading to an increase in adsorption capacity. Pb(II), however, precipitates into $Pb(OH)_2$ as pH exceeds 6.0 [14, 15]. Thus, all adsorption experiments were carried out at pH 5.0.
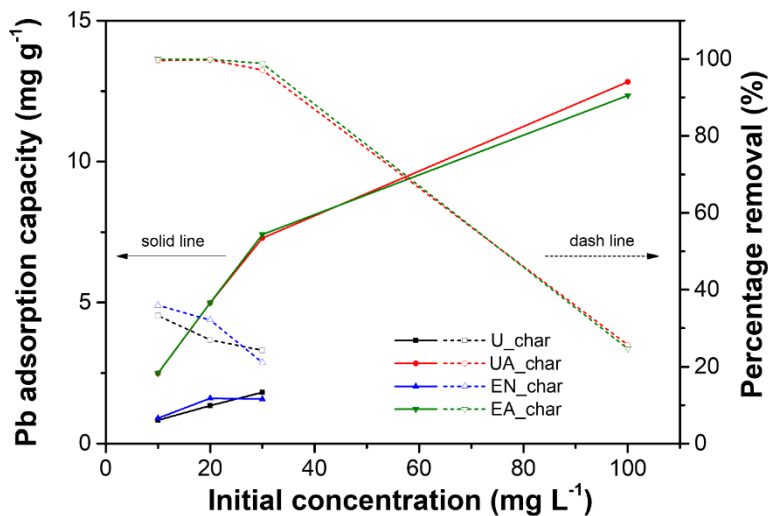
Figure 4. Effect of initial Pb(II) concentration on Pb adsorption capacity in terms of Pb(II) removal percentage for U_char, UA_char, EN_char, and EA_char. Adsorption conditions were 4 g L^{-1} adsorbent and room temperature.

Another essential factor in the adsorption process is the initial concentration metal ions, which affects the equilibrium with the adsorbent [16] and the adsorption rate [17]. Figure 4 shows a clear correlation between adsorption capacities and initial concentrations of Pb(II) for U_char, UA_char, EN_char, and EA_char. Adsorption capacities of all hydrochar samples increased with initial Pb concentrations. The increase in the adsorption capacity from 10 to 30 mg L^{-1} is attributed to transferring of Pb(II) ions into the interior structure of hydrochar facilitated by greater concentration gradients of Pb(II) ions between the solution and the char. At low initial concentration, Pb(II) ions are mainly adsorbed onto the outer surface of hydrochar, resulting in weaker adsorption capacity [8]. The capacities of the U_char and EN_char were identical for initial Pb concentrations from 10 to 30 mg L^{-1}. This indicates that oil extraction had no meaningful impact on Pb(II) adsorption. The adsorption capacity of UA_char was substantially higher: 3.0, 3.7, and 4.0 times higher than U_char at 10, 20, and 30 mg L^{-1} are, respectively. Similarly, the adsorption capability of EA_char was 2.8, 3.1, and 4.7 times greater than that of EN_char at 10, 20, and 30 mg L^{-1} are, respectively. This indicates that more adsorption sites were formed on the surface after CO_2 activation. It is worth noting that the percentages of Pb(II) removal for UA_char and EA_char are close to 100% at low initial Pb(II) concentrations. As the initial concentration increases to 100 mg L^{-1}, the adsorption capacity of UA_char and EA_char reaches 12.83 and 12.34 mg g^{-1}, respectively, whereas their removal ratios decrease to 25.7% and 24.7%, indicating that the adsorption sites on CO_2-activated hydrochar are fully saturated.

Figure 5 shows the linear isotherm plots for Langmuir and Freundlich models, respectively. The values of the Langmuir and Freundlich isotherm parameters with corresponding correlation coefficients (R^2) are summarized in Table 3. R^2 values for the Langmuir model were higher than those for the Freundlich model, indicating that the Langmuir model describes Pb(II) adsorption onto the hydrochars better [18]. Based on the Langmuir parameters, UA_char had the highest Pb(II) adsorption capacity (Table 3).
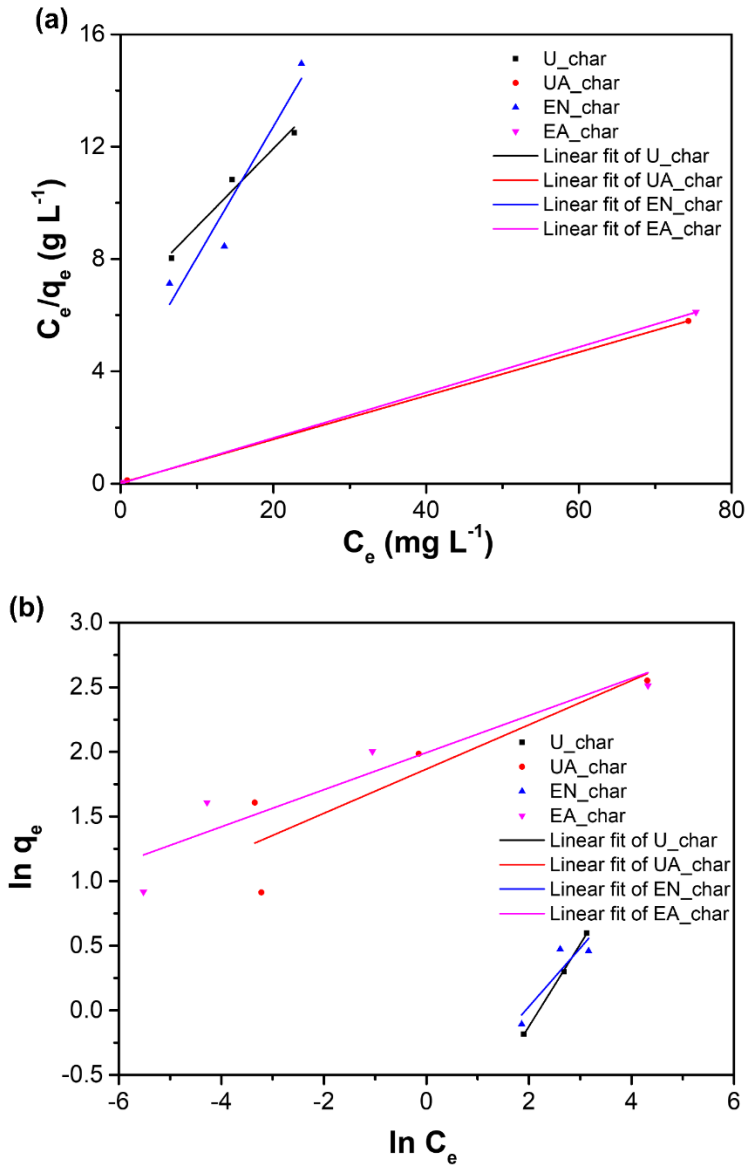
Figure 5. (a) Linear Langmuir isotherm plots, and (b) linear Freundlich isotherm plots for Pb(II) adsorption on U_char, UA_char, EN_char, and EA_char at 25 °C.

Table 3. Langmuir and Freundlich isotherm parameters for Pb(II) adsorption on U_char, UA_char, EN_char, and EA_char at 25 °C.

Sample	Langmuir model			Freundlich model		
	q_m (mg g⁻¹)	K_L (L mg⁻¹)	R^2	n	K_F (mg g⁻¹)	R^2
U_char	3.60	0.04	0.9770	1.57	0.25	0.9994
UA_char	12.88	3.42	0.9999	5.84	6.47	0.7991
EN_char	2.15	0.14	0.9302	2.21	0.42	0.8028
EA_char	12.36	11.19	0.9999	6.97	7.35	0.8752

Considering the greatest adsorption capability observed for UA_char, as well as the potential application of hydrochar in the half-cell of LIBs, Pb-adsorbed UA_char (UAP_char) is chosen as the anode material and assembled in a half-cell configuration. The electrochemical properties of the UAP_char in the voltage range of 0.1-3.0 V are plotted in Figure 6. As depicted in Figure 6(a), the discharge capacities of the 1st, 2nd, 5th, 50th, and 100th cycles were 353.4, 171.3, 163.8, 173.5, and 183.2 mA h g⁻¹ at 0.1 A g⁻¹, respectively. The large capacity loss between the first and the second cycles is ascribed to the inevitable formation of a solid electrolyte interphase (SEI) layer and irreversible lithium insertion into the carbon structure [19, 20], resulting in a low initial Coulombic efficiency of 46.6%. After the first five cycles, however, the Coulombic efficiency remained over 98%, implying the good reversibility for UAP_char as an anode. The current densities increased from 0.1 to 0.2, 0.4, 0.8, 1.6, and 3.2 A g⁻¹ (Figure 6(b)). The specific capacities decreased from 188.8, 161.3, 135.0, 111.3, and 87.5, to 62.5 mA h g⁻¹, and maintained at 175.0 and 198.8 mA h g⁻¹ after recovering to low current densities of 0.2 and 0.1 A g⁻¹, respectively, further demonstrating good anode stability at high rate conditions. The specific capacity had an increasing trend when returning to 0.1 A g⁻¹, compared with the initial low current density (Figure 6(c)). This trend is ascribed to unique biomass structures enhancing the ion accessibility during long-term cycling [20, 21].

(a)
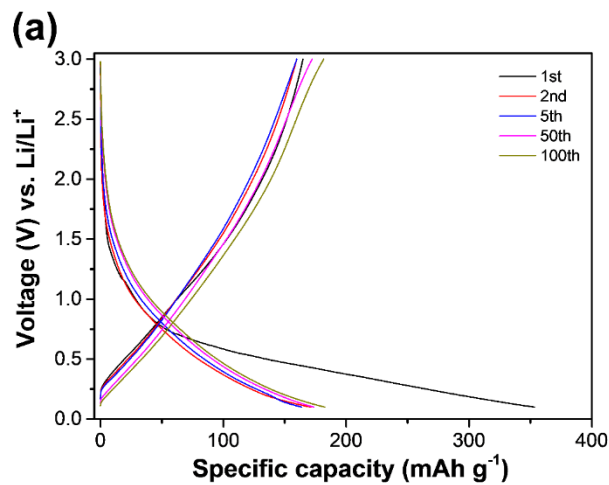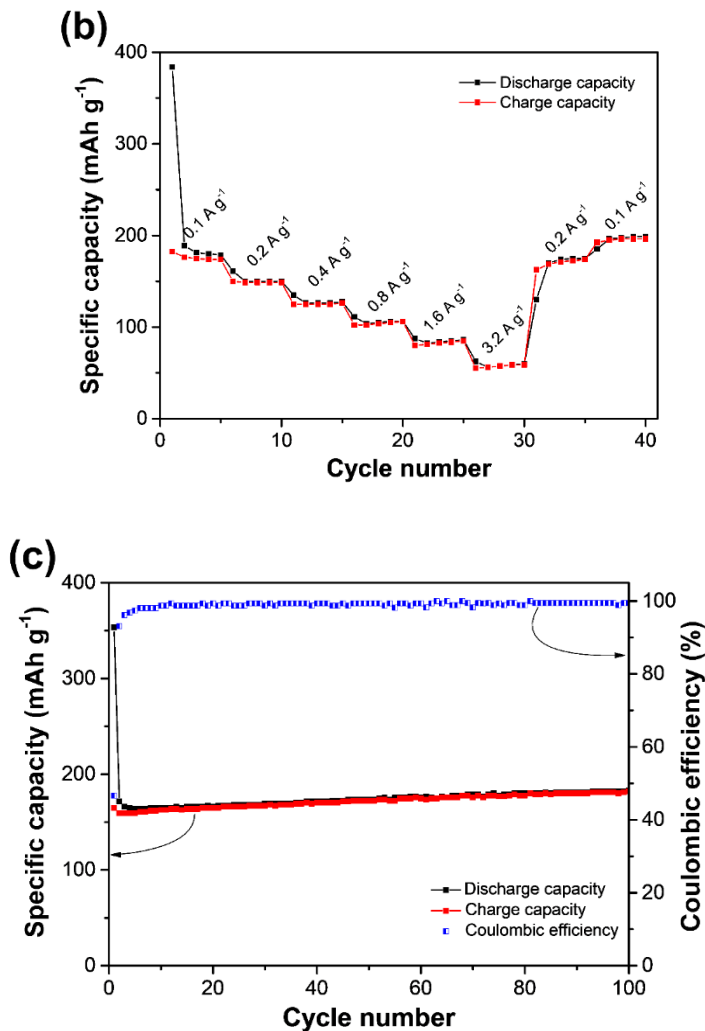
Figure 6. Electrochemical performance of UAP_char in a half-cell LIBs. (a) Galvanostatic discharge/charge voltage profiles for the 1st, 2nd, 5th, 50th, 100th cycle at a current density of 0.1 A g^{-1}; (b) rate capabilities at different current densities (0.1, 0.2, 0.4, 0.8, 1.6, 3.2, and then back to 0.1 A g^{-1}); and (c) cycling performance at 0.1 A g^{-1} with corresponding Coulombic efficiency.

6. Provide a paragraph on who will benefit from your research results. Include any water agency that could use your results.

This work uses hydrochar derived from wastewater-treatment algae as adsorbents which will be further recycled as anodes in LIBs. First, it would be beneficial to the wastewater utilities due to the potential application of wastewater-treatment algae. Second, attributing to the effective adsorption capacity, it provides the preliminary data to other researchers who studying biomass-based adsorbents. Also, the decreased Pb concentration in the groundwater will benefit for the public and environment. Third, battery companies might gain inspiration from recycling of Pb-based hydrochar.

7. **Describe how you have spent your grant funds. Also provide your budget balance and how you will use any remaining funds. If you anticipate any funds remaining after May 31, 2020, please contact Carolina Mijares immediately. (575-646-7991; mijares@nmsu.edu)**

Items	Cost ($)
Graduate Assistant Salary	2, 064.66
Fringe Benefits	20.24
Domestic Travel	90.00
Laboratory Supplies	2070.90
Poster Printing	63.80
Rental	16.85
Laboratory Analysis	1,135.00
Total Expenditures	**5,461.45**
Balance Available	**1,038.55**

8. **List presentations you have made related to the project.**

Poster presentation in NM WRRI 64th Annual New Mexico Water Conference, November 6-8, 2019, Pojoaque, NM

9. **List publications or reports, if any, that you are preparing. For all publications/reports and posters resulting from this award, please attribute the funding to NM WRRI and the New Mexico State Legislature by including the account number: NMWRRI-SG-2019.**

The manuscript is under preparation.

10. **List any other students or faculty members who have assisted you with your project.**

Tianbai Tang (Master student, Department of Chemical & Materials Engineering, NMSU)
Dr. Feng Cheng (Postdoc, Department of Chemical Engineering, Worcester Polytechnic Institute)
Di Huang (Ph.D student, Department of Chemical & Materials Engineering, NMSU)
Dr. Catherine E. Brewer (Faculty, Department of Chemical & Materials Engineering, NMSU)

11. Provide special recognition awards or notable achievements as a result of the research including any publicity such as newspaper articles, or similar.

Not applicable.

12. Provide information on degree completion and future career plans. Funding for student grants comes from the New Mexico Legislature and legislators are interested in whether recipients of these grants go on to complete academic degrees and work in a water-related field in New Mexico or elsewhere.

I'm a Ph.D student and plan to graduate this year. After graduation, I'd like to be a Postdoc.

You are encouraged to include graphics and/or photos in your draft and final report.

Final reports will be posted on the NM WRRI website.

References

[1] X. Li, Z. Wang, Q. Li, J. Ma, M. Zhu, Preparation, characterization, and application of mesoporous silica-grafted graphene oxide for highly selective lead adsorption, Chemical Engineering Journal 273 (2015) 630-637.

[2] Y. Chen, J. Chen, S. Chen, K. Tian, H. Jiang, Ultra-high capacity and selective immobilization of Pb through crystal growth of hydroxypyromorphite on amino-functionalized hydrochar, Journal of Materials Chemistry A 3 (2015) 9843-9850.

[3] J.T. Petrović, M.D. Stojanović, J.V. Milojković, M.S. Petrović, T.D. Šoštarić, M.D. Laušević, M.L. Mihajlović, Alkali modified hydrochar of grape pomace as a perspective adsorbent of Pb^{2+} from aqueous solution, Journal of Environmental Management 182 (2016) 292-300.

[4] Y. Hu, S. Wang, J. Li, Q. Wang, Z. He, Y. Feng, A.E.-F. Abomohra, S. Afonaa-Mensah, C. Hui, Co-pyrolysis and co-hydrothermal liquefaction of seaweeds and rice husk: Comparative study towards enhanced biofuel production, Journal of Analytical and Applied Pyrolysis 129 (2018) 162-170.

[5] I. Langmuir, The adsorption of gases on plane surfaces of glass, mica and platinum, Journal of the American Chemical Society 40 (1918) 1361-1403.

[6] K.Y. Foo, B.H. Hameed, Insights into the modeling of adsorption isotherm systems, Chemical Engineering Journal 156 (2010) 2-10.

[7] M. Matouq, N. Jildeh, M. Qtaishat, M. Hindiyeh, M.Q. Al Syouf, The adsorption kinetics and modeling for heavy metals removal from wastewater by Moringa pods, Journal of Environmental Chemical Engineering 3 (2015) 775-784.

[8] Z. Liu, F.-S. Zhang, Removal of lead from water using biochars prepared from hydrothermal liquefaction of biomass, Journal of Hazardous Materials 167 (2009) 933-939.

[9] M. Parsa, M. Nourani, M. Baghdadi, M. Hosseinzadeh, M. Pejman, Biochars derived from marine macroalgae as a mesoporous by-product of hydrothermal liquefaction process: Characterization and application in wastewater treatment, Journal of Water Process Engineering 32 (2019) 100942.

[10] T.-H. Liou, Preparation and characterization of nano-structured silica from rice husk, Materials Science and Engineering: A 364 (2004) 313-323.

[11] Y. Niu, R. Qu, C. Sun, C. Wang, H. Chen, C. Ji, Y. Zhang, X. Shao, F. Bu, Adsorption of Pb (II) from aqueous solution by silica-gel supported hyperbranched polyamidoamine dendrimers, Journal of Hazardous Materials 244 (2013) 276-286.

[12] M. Kılıc, Ç. Kırbıyık, Ö. Çepelioğullar, A.E. Pütün, Adsorption of heavy metal ions from aqueous solutions by bio-char, a by-product of pyrolysis, Applied Surface Science 283 (2013) 856-862.

[13] I. Kula, M. Uğurlu, H. Karaoğlu, A. Celik, Adsorption of Cd (II) ions from aqueous solutions using activated carbon prepared from olive stone by $ZnCl_2$ activation, Bioresource Technology 99 (2008) 492-501.

[14] J.-X. Yu, L.-Y. Wang, R.-A. Chi, Y.-F. Zhang, Z.-G. Xu, J. Guo, Competitive adsorption of Pb^{2+} and Cd^{2+} on magnetic modified sugarcane bagasse prepared by two simple steps, Applied Surface Science 268 (2013) 163-170.

[15] L. Lv, M.P. Hor, F. Su, X. Zhao, Competitive adsorption of Pb^{2+}, Cu^{2+}, and Cd^{2+} ions on microporous titanosilicate ETS-10, Journal of Colloid and Interface Science 287 (2005) 178-184.

[16] M.A. Hanif, R. Nadeem, H.N. Bhatti, N.R. Ahmad, T.M. Ansari, Ni (II) biosorption by Cassia fistula (Golden Shower) biomass, Journal of Hazardous Materials 139 (2007) 345-355.

[17] N. Ahalya, R. Kanamadi, T. Ramachandra, Biosorption of chromium (VI) from aqueous solutions by the husk of Bengal gram (Cicer arientinum), Electronic Journal of Biotechnology 8 (2005) 0-0.

[18] S.E. Elaigwu, V. Rocher, G. Kyriakou, G.M. Greenway, Removal of Pb^{2+} and Cd^{2+} from aqueous solution using chars from pyrolysis and microwave-assisted hydrothermal carbonization of Prosopis africana shell, Journal of Industrial and Engineering Chemistry 20 (2014) 3467-3473.

[19] F. Gao, C. Geng, N. Xiao, J. Qu, J. Qiu, Hierarchical porous carbon sheets derived from biomass containing an activation agent and in-built template for lithium ion batteries, Carbon 139 (2018) 1085-1092.

[20] J. Hou, C. Cao, F. Idrees, X. Ma, Hierarchical porous nitrogen-doped carbon nanosheets derived from silk for ultrahigh-capacity battery anodes and supercapacitors, ACS Nano 9 (2015) 2556-2564.

[21] Z.-S. Wu, Y. Sun, Y.-Z. Tan, S. Yang, X. Feng, K. Müllen, Three-dimensional graphene-based macro-and mesoporous frameworks for high-performance electrochemical capacitive energy storage, Journal of the American Chemical Society 134 (2012) 19532-19535.